



1 **A new criterion for determining the representative elementary volume of**
2 **translucent porous media and inner contaminant**

3 Ming Wu^{1,2}, Jianfeng Wu^{2*}, Jichun Wu², and Bill X. Hu^{1*}

4

5 ¹ Institute of Groundwater and Earth Sciences, Jinan University, Guangzhou 510632,
6 China

7 ²Key Laboratory of Surficial Geochemistry, Ministry of Education; Department of
8 Hydrosiences, School of Earth Sciences and Engineering, Nanjing University, Nanjing
9 210023, China

10 *Correspondence to:* J.F. Wu (jfwu@nju.edu.cn), B.X. Hu (billhu@jnu.edu.cn)

11



12 **ABSTRACT**

13 Representative elementary volume (REV) is essential to measure and quantify the
14 effective parameters of a complex heterogeneous medium. Since previous REV estimation
15 criteria having multiple limitations, a new criterion (χ^i) is proposed to estimate REV of a
16 translucent material based on light transmission techniques. Two sandbox experiments are
17 performed to estimate REV of porosity, density, tortuosity and perchloroethylene (PCE)
18 plume using multiple REV estimation criteria. In comparison with χ^i , previous REV
19 estimation criteria based on the coefficient of variation (C_v^i), the entropy dimension
20 (DI^i) and the relative gradient error (ϵ_g^i) are tested in REV quantification of translucent
21 silica and inner PCE plume to achieve their corresponding effects. Results suggest that
22 new criterion (χ^i) can effectively identify the REV in the materials, whereas the
23 coefficient of variation (C_v^i) and entropy dimension (DI^i) cannot. The relative
24 gradient error (ϵ_g^i) can make the REV plateau obvious, while random fluctuations make
25 the REV plateau uneasy to identify accurately. Therefore, the new criterion is
26 appropriate for REV estimation for the translucent materials and inner contaminant.
27 Models are built based on Gaussian equation to simulate the distribution of REV for
28 media properties, which frequency of REV is dense in the middle and sparse on both sides.
29 REV estimation of PCE plume indicates high level of porosity lead to large value of
30 mean and standard deviation for REV of PCE saturation (S_0) and PCE-water interfacial
31 area (A_{ow}). Fitted equations are derived for distribution of REV for PCE plume related to
32 d_m (distances from mass center to considered point) and d_l (distances from injection



33 position to considered point). Moreover, relationships between REV_s of PCE plume and
34 S_o are fitted using regression analysis. Results suggest a decreasing trend appears for
35 S_o -REV when S_o increases, while A_{ow} -REV increases with increasing of S_o .

36 **Keywords:** new criterion; representative elementary volume (REV); translucent material

37 1. Introduction

38 Modelling groundwater and contaminant (such as hazardous irons) transport in
39 subsurface environment is based on the premise that micro-structure of aquifer exist a
40 representative elementary volume (REV) (Wang et al., 2016; Lei and Shi, 2019). REV act
41 as a micro-scale characteristic, which is important to improve our understanding of
42 materials, inner fluid flow and other processes (Brown and Hsieh, 2000;
43 Costanza-Robinson et al., 2011; Wu et al., 2017). Previous studies suggested that even the
44 Platinum-Nanoparticle-Catalyzed hydrogenation reactions and ion transport through
45 angstrom-scale slits in cell activity existed apparent size effect, implying size effect is a
46 wide characteristic for many process and materials (Bai et al., 2016; Esfandiar et al., 2017).
47 With the help of REV, a porous medium can be treated as continuum medium (Brown and
48 Hsieh, 2000; Kang et al., 2003; Müller and Siegesmund, 2010; Teruel and Rizwan-uddin,
49 2010; Hendrick et al., 2012; Wang et al., 2012; Ukrainczyk and Koenders, 2014; Kim and
50 Mohanty, 2016; Gilevska et al., 2019). A conceptual representation of “REV curve”,
51 characterizing porosity (n) change with measured scale (L) increment, is presented in Fig.
52 1c. Based on the characteristic of REV curve in Fig. 1c, the REV curve can be divided into
53 three regions. When measured scale is in region I, the porosity fluctuates drastically at
54 small scales. As measured scale size ranging between L_{min} and L_{max} , a flat plateau with



55 constant and steady value is encountered and the property is factored into its average value.
56 Material property in spatial scales less than L_{min} is spatially varied portions with small
57 scale, which can be easily influenced by individual pores in micro-structure such as region
58 I (Fig. 1c). Likewise, material property is allowed drift to new values in spatial scale
59 above L_{max} due to additional morphological structures of large field heterogeneity (region
60 III). As a matter of fact, REV scale of region II can be derived between the small and
61 spatially varied property in region I and large field variability in region III. However, the
62 lower and upper boundaries L_{min} and L_{max} of REV plateau is hard to be identified in reality
63 (Brown and Hsieh, 2000; Costanza-Robinson et al., 2011).

64 As technology advanced and progressed, non-destructive and non-invasive
65 techniques of x-ray and gamma ray micro-tomography were utilized for micro-structure
66 characteristic measurement in materials (Ghilardi, 1993; Brown and Hsieh, 2000;
67 Niemet and Selker, 2001; Bob et al., 2008; Al-Raoush and Papadopoulos, 2010;
68 Costanza-Robinson et al., 2011; Al-Raoush, 2012; Borges and Pires, 2012; Fernandes et
69 al., 2012; Rozenbaum and Roscoat, 2014; Pereira Nunes et al., 2016; Piccoli et al., 2019).
70 Generally, REV estimation also was usually implemented by micro visualization and
71 scanning of X-ray and gamma ray in laboratory (Brown and Hsieh, 2000; Razavi et al.,
72 2007; Nordahl and Ringrose, 2008; Al-Raoush and Papadopoulos, 2010;
73 Costanza-Robinson et al., 2011; Rozenbaum and Roscoat, 2014; Borges et al., 2018),
74 while different criteria were utilized to quantify REV (Brown and Hsieh, 2000; Martínez
75 et al., 2007; Nordahl and Ringrose, 2008; Costanza-Robinson et al., 2011). Lower
76 boundary scale L_{min} of REV was identified by means of entropy dimension (DI^i) for eight



77 soil samples (Martínez et al., 2007). Further, REV scale of permeability for ripple
78 laminated sandstone intercalated with mudstone was estimated using the coefficient of
79 variation (C_v^i), which the REV scale is identified by the variability among the ten
80 samples to achieve average REV scale (Nordahl and Ringrose, 2008). As a result, only
81 one REV boundary was identified and not every sample can be estimated effectively
82 (Nordahl and Ringrose, 2008). More interestingly, REV scales for porosity, moisture
83 saturation and air-water interfacial areas in porous media were estimated by a criterion
84 named the relative gradient error (ϵ_g^i) (Costanza-Robinson et al., 2011). In summary, the
85 REV estimation was made by multiple kinds of criteria, while the REV identification
86 effects of these criteria were not clear.

87 In this study, a new criterion (χ^i) for REV estimation is proposed to identify the REV
88 scale of the translucent silica and inner contaminant. Two perchloroethylene (PCE)
89 transport experiments are conducted in two dimensional (2D) sandboxes to test the effect
90 of different REV estimation criteria. Translucent silica is selected for associated REV
91 analysis due to its extensive utilization in laboratory experiment of exploring groundwater
92 flow and contaminant migration behavior in micro-structure of a sandy aquifer (Niemet
93 and Selker, 2001; Bob et al., 2008; Costanza-Robinson et al., 2011). Moreover, translucent
94 silica is also an important material applied in numerous industries (Bouvry et al., 2016). In
95 laboratory experiments, translucent silica is packed in 2D sandboxes where porosity,
96 density, tortuosity, PCE saturation are derived by light transmission technique (Fig. 1a).
97 Porosity and PCE saturation are selected as the representative variables to explore
98 corresponding REV estimation by different criteria, which is very essential and significant



99 for REV identification. Previous criteria such as the coefficient of variation (C_v^i),
100 entropy dimension (DI^i), the relative gradient error (ϵ_g^i) and the new criterion- χ^i are
101 tested in REV estimation. Associated effects are analyzed to achieve the best criterion of
102 effective and appropriate quantification of REV.

103 2. Experiment procedure and method

104 2.1 Experiment

105 Two sandboxes (Fig. 2a and b) packed by translucent silica medium are prepared in
106 laboratory to test different criteria of REV quantification. PCE is selected as a typical
107 DNAPL contaminant used in experiments. 2D sandbox is composed by three aluminum
108 interior frames and two glass walls, which thickness is 1.6cm. The dimensions of
109 sandboxes used in Experiments-I and II are 20 (width) \times 15 (height) and 60 (width) \times 45
110 (height) F40/50 and F20/30 mesh translucent silica sands are used for background material
111 for Experiments-I and II. To make the translucent silica fully saturated by water in a flow
112 field close to natural groundwater environment (Erning et al., 2012), water flow at flow
113 velocity of 0.5 m/d is set from left to right in laboratory sandbox experiments (Fig. 2a and
114 b). Water is restricted in a sandbox that the top and bottom layers of sandbox are packed
115 by F70/80 mesh translucent silica as capillary barriers. Light source is placed behind the
116 sandbox to make light penetrate through translucent media and capture emergent light
117 intensity using a thermoelectrically air-cooled charge-coupled device (CCD) camera (Fig.
118 1a). Afterward, PCE is injected into sandboxes from the injection needle at constant rate
119 of 0.5 mL /min for two experiments. Detailed experimental conditions are listed in Table1.



120 2.2 Light transmission techniques

121 By means of light transmission technique (Fig. 1a), DNAPL and water saturation can
122 be obtained rapidly and in real-time, which greatly help to explore mechanism of
123 groundwater flow and contaminant migration in porous media. When light passes through
124 translucent materials of a given thickness, the emergent light intensity after the absorptive
125 and interfacial losses can be expressed as (Niemet and Selker, 2001; Bob et al., 2008; Wu
126 et al., 2017):

$$127 \quad I_T = CI_0(\prod \tau_j) \exp(-\sum \alpha_i d_i) \quad (1)$$

128 where I_0 is the original light intensity; C is a constant of correction for light emission
129 and light observation; τ_j is the transmittance when light penetrate from phase i to $i+1$;
130 α_i is the absorption coefficient when light penetrate in phase i ; d_i is the length of light
131 penetration path in phase i .

132 To derive the porosity, the 2D translucent porous medium should be only saturated
133 by water. Consequently, the emergent light intensity can be expressed as:

$$134 \quad I_s = CI_0 \tau_{s,w}^{2k_o} \exp(-\alpha_s k_s d_s) \quad (2)$$

135 where $\tau_{s,w}^{2k_o}$ is the transmittance of solid-water interface; α_s is solid particles
136 absorption coefficient; d_s is median diameter of the solid particles; k_o is the number of
137 pores across light penetration path; k_s is the number of solid particles across light
138 penetration path.

139 If we arbitrarily select an infinitesimal element, its area A_o approaches zero
140 ($A_o \rightarrow 0$) from the 2D translucent porous media (Fig. 1b), and suppose the infinitesimal
141 element with thickness L_T containing solid particles and pores that can be regarded as



142 lamellar structure (Fig. 1c), we can obtain the following relationships:

143
$$\theta A_o L_T = A_o k_o d_o \quad (3)$$

144
$$k_s d_s + k_o d_o = L_T \quad (4)$$

145 where d_o is the median diameter of pores; θ is porosity.

146 Substituting Eq. (3) and Eq. (4) into Eq. (2), the relationship between emergent
147 light intensity and porosity can be achieved (Wu et al., 2017):

148
$$\ln I_s = \beta + n\gamma \quad (5)$$

149 where $\beta = \ln\left(\frac{CI_s}{e^{\alpha_s d_s L_T}}\right)$ and $\gamma = \ln\left(\tau_{s,w}^{\frac{2L_s}{d_o}} e^{\alpha_s L_T}\right)$. β and γ can be determined from
150 experimental data, then porosity can be obtained.

151 The density and tortuosity are derived as (Wu et al., 2018):

152
$$\rho = \theta\rho_w + (1.0 - \theta)\rho_s \quad (6)$$

153
$$\tau = 1 + \frac{\pi - 2}{\sqrt{\frac{\pi}{1 - \theta}}} \quad (7)$$

154 where ρ is the density of translucent porous media; ρ_w is the density of water; ρ_s is the
155 density of solid particles; τ is tortuosity .

156 The saturation of dense nonaqueous phase liquid (DNAPL) was quantified by light
157 transmission technique based on light pass through translucent materials (Niemet and
158 Selker, 2001; Bob et al., 2008):

159
$$S_o = \frac{\ln I_s - \ln I_T}{\ln I_s - \ln I_{oil}} \quad (8)$$

160 where S_o is the saturation of DNAPL; I_s is the light intensity after light penetration
161 through translucent porous when all pores are fully saturated by water; I_{oil} is the light
162 intensity when all pores are fully saturated by DNAPL; I_T is the light intensity after



163 penetration through translucent materials. After quantification of PCE saturation,
164 PCE-water interfacial area (A_{ow}) can be obtained based on the method proposed by Wu et
165 al. (2017), where the unit of A_{ow} is cm^{-1} .

166 2.3 Criteria of REV quantification

167 The REV is defined as the volume range in which all material characteristics are
168 factored into the average and associated values approach single and constant (Brown
169 and Hsies, 2000). In the range of REV, the value of one associated property will meet
170 the condition:

$$171 \quad \frac{\partial Y(L_i)}{\partial L} \Big|_{L_i=L_o} = 0 \quad (9)$$

172 where the $Y(L_i)$ is the value of an associated property when system scale is L_i ; L_i is the
173 value of system scale; L_o is the scale range of REV, $L_{\min} < L_o < L_{\max}$; L_{\max} is upper
174 boundary of REV; L_{\min} is lower boundary of REV scale. According to the Eq. (9),
175 when the measured scale (L_i) reaches REV range, the derivative $\frac{\partial Y(L_i)}{\partial L} \rightarrow 0$ will tend
176 to zero. As a matter of fact, most previously used criteria were applied to estimate REV
177 based on this requirement. The REV estimation criteria tested in this study are
178 illustrated in Table 2.

179 To evaluate the REV of porosity, the coefficient of variation (C_v^i) (Table 2) is
180 utilized to estimate the variability (Nordahl and Ringrose, 2008):

$$181 \quad C_v^i = \frac{\hat{s}_i}{\varphi_i} \quad (10)$$

182 where i is the cuboid window (Fig. 1b) increment number; φ is the measured variable,
183 such as porosity; \hat{s}_i is the standard deviation of sub-grids' variable in different



184 measured volume or scale; $\bar{\varphi}_i$ is the arithmetic average of the variable values in the
 185 sub-grids. When number of sub-grids (N) is less than 10, a correction is utilized to
 186 replace Eq. (10). According to Nordahl and Ringrose (2008), $0 < C_V^i < 0.5$ is defined
 187 as homogeneous and $C_V^i = 0.5$ can be used as criterion to identify the REV scale.

188 Similarly, for porosity of translucent silica, entropy dimension (DI^i) (Table 2) is
 189 utilized for REV analysis and estimation (Martínez et al., 2007), which is defined as:

$$190 \quad DI^i \approx \frac{\sum_{j=1}^{m(i)} \mu_j(L_\varepsilon) \log \mu_j(L_\varepsilon)}{\log L_\varepsilon} \quad (11)$$

191 where, L_ε is the scale of sub-grid; “ \approx ” indicates the asymptotic equivalence as $L_\varepsilon \rightarrow 0$
 192 (Martínez et al., 2007); j is the ordinal number of sub-grid in measured cuboid window
 193 (Fig. 1b) of increment number i ; $m(i)$ is the total number of sub-grids in measured
 194 cuboid window (Fig. 1b) of increment number i ; $\mu_j(\varepsilon)$ is the proportion of the
 195 variable of sub-grid j in the whole measured cuboid window i . The right hand side of Eq.
 196 (11) is the simplification of Shannon entropy of all sub-grids, in which DI^i can be
 197 considered as the average of logarithmic values of the variable distribution weighted by
 198 $\mu_j(L_\varepsilon)$ to quantify the degree of medium heterogeneity. Using Eq. (11), a series of values
 199 of DI^i ($i=1,2,3,\dots$) are obtained for each measured cuboid window (Fig. 1b) of
 200 increment number i . For estimation of the REV in a porous medium, the relative
 201 increment of entropy dimension and associated criterion of REV identification are
 202 respectively expressed as:

$$203 \quad RI^i = \left| \frac{DI^j - DI^{j-1}}{DI^{j-1}} \right| \times 100 \quad (12)$$

$$204 \quad RI^i \leq 0.2 CV_{DI} \quad (13)$$

205 where CV_{DI} is the coefficient of variation of DI^i series ($i=1,2,3,\dots$), which is



206 calculated through $CV_{DI} = (\hat{s}_{DI} / \overline{DI}) \times 100$; \overline{DI} is the mean value of the DI^i series;
207 \hat{s}_{DI} is the standard deviation of the DI^i series.

208 To achieve the REV for multiple system variables, such as porosity, moisture
209 saturation and air-water interfacial areas in an unsaturated porous medium, a criterion
210 named the relative gradient error (Table 2) was applied (Costanza-Robinson et al., 2011):

$$211 \quad \varepsilon_g^i = \left| \frac{\varphi^{i+1} - \varphi^{i-1}}{\varphi^{i+1} + \varphi^{i-1}} \right| \frac{1}{\Delta L} \quad (14)$$

212 where ε_g^i is relative gradient error; ΔL is the measured cuboid window size increment
213 length for REV estimation. Usually, ε_g^i less than 0.2 (Costanza-Robinson et al., 2011) is
214 utilized to identify a REV sizes.

215 A new criterion based on the required condition of REV is proposed to estimate
216 the REV range for the translucent silica in this study:

$$217 \quad \chi^i = \frac{|\delta_{i+1} - \delta_{i-1}|}{\delta_i \Delta L} \quad (15)$$

218 where δ^i is the dimensionless range, $\delta^i = \frac{\phi(L_i)_{\max} - \phi(L_i)_{\min}}{\overline{\phi(L_i)}}$; $\phi(L_i)_{\max}$ is the
219 maximum value of the variable on the volume scale L_i ; $\phi(L_i)_{\min}$ is the minimum value
220 of the variable on the volume scale L_i ; $\overline{\phi(L_i)}$ is the mean value of the variable on the
221 volume scale L_i . Brown and Hsieh (2000) suggested $\delta^i = \frac{\phi(L_i)_{\max} - \phi(L_i)_{\min}}{\overline{\phi(L_i)}} \ll 1$ can
222 be used for REV estimation. In fact, the calculated value of δ^i mostly is less than 1,
223 while $\delta^i \ll 1$ is hard to be used to identify the REV scale for realistic materials, such
224 as the translucent silica used in this study. The value limit of χ^i used for REV estimation
225 also is explored in this study.



226 In this study, criteria for the coefficient of variation (C_v^i), entropy dimension
227 (DI^i), the relative gradient error (ϵ_g^i) and the new criterion (χ^i) are all applied in REV
228 estimation for porosity and PCE saturation. Corresponding REV plateau identification
229 effects are compared to select the best criterion for REV quantification.

230 3. Results and discussion

231 3.1 REV identification effect of different criteria

232 3.1.1 The coefficient of variation

233 Emergent light intensity distributions of translucent silica for two experiments, which
234 had been fully saturated by water, was obtained by a thermoelectrically air-cooled
235 charge-coupled device (CCD) camera (Niemet and Selker, 2001; Bob et al., 2008). The
236 porosity, density, tortuosity and PCE saturation for two experiments are derived by light
237 transmission technique as shown in Figs. 3a and b. The PCE spreads from the injecting
238 point shaped like a drop of water at $t=1.44$ min (Fig. 3b). In 2D sandboxes for two
239 experiments, PCE plume infiltrates in translucent silica sands infiltration paths and PCE
240 plumes reach the bottom after $t=80$ min.

241 Every pixel with small scale could be approximated as infinitesimal element in high
242 resolution image to apply light transmission techniques. As consequence, porosity of
243 translucent silica was derived with light transmission technique through Eq. (5) (Fig. 2c).
244 The whole 2D translucent silica area was numerically discretized that every cell had the
245 uniform dimensions of $0.015\text{m}\times 0.015\text{m}$. The cuboid window (Fig. 1d) was utilized to
246 quantify the variables (porosity, density, tortuosity, PCE saturation, PCE-water interfacial
247 area) of every cell as measured scale was increased. In detail, the measured cuboid



248 window scale was increased from the center of each cell and associated value of variable
249 was calculated from the high resolution porosity of 2D translucent silica derived by light
250 transmission technique. Observation cells were selected from the discretized cells (Fig. 3b)
251 of which the cells I-1~2 and II-1~2 belong to Experiments-I and II, respectively. Porosity
252 and PCE saturation variation curves of these observation cells with increasing measured
253 cuboid window scale were shown in Fig. 4a and b. However, for all observation cells from
254 translucent silica, the REV plateaus were not obvious to be objectively judged visually,
255 which made REV plateaus hard to identify effectively by original variation curves for
256 porosity and PCE saturation (Figs. 4a and b).

257 To make the REV plateau more explicit, different criteria of REV quantification
258 are utilized. The coefficient of variation (C_V^i) of porosity and PCE saturation fluctuating
259 with increase of measured cuboid window size is shown in Fig. 4. The measured cuboid
260 window scale is limited to the dimensions of cells in discretization of 2D translucent
261 silica. The observation cells show various characteristics of variation tendency for the
262 coefficient of variation (C_V^i). The θ and S_o variation curves of coefficient of variation (C_V^i)
263 for all observation cells do not reach stable values as those shown in Figs. 4a and b, the
264 beginning of the REV flat plateau is not easy to identify, the coefficient of variation (C_V^i)
265 is not suitable for REV estimation. According to the heterogeneity definition by Corbett
266 and Jensen (1992), the heterogeneity of materials is defined by C_V^i magnitude that
267 $0 < C_V^i < 0.5$ is classed as homogeneous medium, $0.5 < C_V^i < 1.0$ is classed as
268 heterogeneous medium and $1.0 < C_V^i$ is classed as strong heterogeneous medium. For
269 the coefficient of variation (C_V^i) magnitude in Figs. 4a-f, the C_V^i values are all below



270 0.5 that the criterion $C_V^i = 0.5$ is unable to identify the REV scale for translucent
271 silica.

272 3.1.2 Entropy dimension

273 Entropy dimension (DI^i) is utilized by Martínez et al. (2007) for multifractal
274 analysis of a porous medium porosity and REV estimation. In this study, entropy
275 dimension (DI^i) is tested to avoid unclear REV plateau in porosity curves. The entropy
276 dimension (DI^i) of porosity is calculated by Eq. (11). Variation curves of entropy
277 dimension (DI^i) for all observation cells (Fig. 2a) are presented in Fig. 4. The curves of
278 entropy dimension (DI^i) of porosity and PCE saturation generally result in the increasing
279 trend curves which makes REV estimates become very difficult and invalid. Entropy
280 dimension (DI^i) was quickly increased with increasing of measured cuboid window size.
281 Compared to the coefficient of variation (C_V^i) of porosity and PCE saturation, entropy
282 dimension (DI^i) increased step by step without opposite fluctuation tendency in the
283 variation curves as length scale of measured cuboid window increased simultaneously. In
284 general, REV plateau in region II (Fig. 1c) of porosity is not obvious for the entropy
285 dimension (DI^i) curves of all observation cells from two experiments, which suggests
286 REV scales is uneasy to identify for translucent silica using entropy dimension (DI^i) by
287 light transmission technique.

288 3.1.3 The relative gradient error

289 The relative gradient error (ε_g^i) of porosity and PCE saturation is calculated by Eq.
290 (14). The variation of ε_g^i at different measured cuboid window scales are shown in Fig.



291 4 for all observation cells in the 2D translucent silica. For all ε_g^i curves at observation
292 cells from experiments, the REV plateaus in region II (Fig. 1a) are more clear than the
293 variation curves based on the criteria of C_V^i and DI^i . Apparently, erratic variations of
294 the relative gradient error (ε_g^i) at small measured cuboid window scales are observed
295 for all ε_g^i curves as the characteristic of REV region I in Fig. 1c. When measured
296 cuboid window scale further increases for all observation cells, the variability and
297 magnitude of the relative gradient error (ε_g^i) decrease well and factored into average,
298 which can be identified as REV plateau in region II (Fig. 1c). The relative gradient error
299 (ε_g^i) makes the REV plateau quantification convenient for all observation cells. At the
300 measured cuboid window size above the REV plateau, ε_g^i curves result in large
301 variability for observation cells I-1~2. These findings suggest that that the relative
302 gradient error (ε_g^i) can make the REV plateau more obvious, which greatly contribute
303 to convenient and applicable REV quantification for translucent silica by light
304 transmission technique. However, random fluctuations exist in ε_g^i curves visually,
305 which make the REV plateau uneasy to identify accurately.

306 3.1.4 The new criterion (χ^i)

307 χ^i of porosity and PCE saturation changing with measured cuboid window size is
308 shown in Fig. 4. Like the region I (Fig. 1c), erratic and random fluctuations appears at
309 small measured cuboid window sizes and χ^i increases with the increase of the measured
310 cuboid window size. When measured scale increases, the values of χ^i for all observation
311 cells appear fast reduction and rapidly tend to steady, which exhibit the characteristic of
312 REV plateau as measured scale reaches region II. The χ^i for observation cells restore the



313 erratic variation state of increasing trend after measured cuboid window size exceeding the
314 REV plateau. As shown in the variation curves of χ^i for all observation cells, the beginning
315 of the REV flat plateaus can be identified easily, suggesting χ^i is more convenient and
316 reliable than other methods for REV estimation. All observation cells show similar
317 variation curves of χ^i that low value intervals are quite apparent, indicating that χ^i is very
318 effective to make the REV plateau obvious for translucent silica used in this study. Using
319 the criterion of χ^i , the REV plateau of region II is flat, which is easily identified,
320 compared with other criteria for observation cells (Figs. 4a and b).

321 3.2 REVs of material properties

322 Based on the REV plateau identifications using the coefficient of variation
323 (C_v^i), entropy dimension (DI^i), the relative gradient error (ε_g^i) and the proposed new
324 criterion χ^i in Figs. 4a and b, the new criterion χ^i appears to be the most appropriate
325 criterion for REV plateau identification. Even though the relative gradient error (ε_g^i) can
326 also make REV plateau obvious, but various random fluctuations weaken the method and
327 reduce the associated accuracy. Therefore, REVs of porosity, density, tortuosity and PCE
328 plume are estimated using the new criterion χ^i in the following study.

329 In fact, large number of discretized cells in the 2D translucent silica for two
330 experiments are quantified using the new criterion χ^i , which is convenient to examine the
331 regularities for REV sizes and related factors. Using the new criterion χ^i , the REV
332 estimation is conducted based on Eq. (15). Fig. 5a shows minimum REV sizes of porosity,
333 density and tortuosity quantified by χ^i for all cells of two experiments. Associated
334 statistical analysis for REVs is illustrated in Fig. 5b, where circular points represent



335 frequency and triangular points represent cumulative frequency. Frequency of REV's is
336 dense in the middle and sparse on both sides, so the distribution of REV's can be fitted by
337 Gaussian equation:

$$338 \quad F = \omega + \frac{1}{\sqrt{2\pi}\delta} e^{-\frac{(REV-v)^2}{2\delta^2}} \quad (16)$$

339 where F is the frequency of REV; ω , δ and v are fitted parameters of the model.

340 After regression analysis, the derived models for REV frequency are listed in Table 3.
341 The coefficients of determination (R^2) of models for REV's of porosity and density all
342 exceed 0.93. R^2 for REV of tortuosity for two experiments exceed 0.7. Moreover, the
343 computed cumulative frequency based on models fit cumulative frequency from
344 experimental results well in Fig. 5b.

345 The minimum REV size frequency for porosity appears a peak between 4.0 mm and
346 5.0 mm for Experiment-I. As minimum REV size of porosity increases, corresponding
347 frequency continuously decreases. Further, smooth convex shape of cumulative frequency
348 is observed for minimum REV size of porosity (Fig. 5b). Most minimum REV sizes of
349 translucent silica distributed in 0.0-7.0mm. For density of translucent silica sand,
350 associated REV frequency appear high values between 2.0~3.0 mm. For the REV sizes of
351 tortuosity, minimum REV sizes distribute in 0.0~6.0 mm. Compared with Experiment-I
352 (F40/50 mesh translucent silica sand), the frequency of REV for Experiment-II (F20/30
353 mesh translucent silica sand with larger porosity) show flat shape and has larger value of
354 standard deviation, especially for REV of porosity. Fig. 5b shows that translucent silica
355 with larger porosity will achieve border distribution of minimum REV sizes distribution
356 compared to translucent silica with relative lower porosity. The mean REV sizes of



357 porosity, density and tortuosity for Experiment-I are 4.35 mm, 2.89 mm and 3.65 mm,
358 respectively. All mean REV sizes of these variables for Experiment-II are larger than
359 REVs of Experiments-II, which corresponding mean REV sizes are 8.05 mm, 2.97 mm
360 and 4.30 mm. These results suggest translucent porous media with higher porosity lead to
361 larger values of mean and standard deviation for REV sizes.

362 3.3 REVs of S_o and A_{ow} for PCE plume

363 The minimum REV sizes of S_o and A_{ow} obtained using new criterion χ^i are shown in
364 Figs. 6a and b. To analyze the regularity of REV distribution for PCE plume, the mass
365 center coordinate of PCE plume for two experiments are quantified for Experiments-I and
366 II. The mass center coordinate are calculated as:

$$367 \quad x_m = \frac{M_{10}}{M_{00}} \quad (17)$$

$$368 \quad z_m = \frac{M_{01}}{M_{00}} \quad (18)$$

369 where x_m is x coordinate of mass center for PCE plume; z_m is z coordinate of mass center
370 for PCE plume; M_{00} , M_{10} and M_{01} are computed using definition of spatial moment (M_{ij}),
371 $M_{ij} = \int_{x_0}^{x_1} \int_{z_0}^{z_1} \theta(x, z) S_o(x, z, t) x^i z^j d_x d_z$; x_0 and z_0 are minimum limits of x axis and z axis; x_1
372 and z_1 are maximum limits of x axis and z axis; $\theta(x, z)$ is the porosity at point (x, z) ; $S_o(x, z, t)$
373 is PCE saturation of point (x, z) at time t.

374 The mass center coordinate of PCE plume derived by Eq. (18) is shown in Fig. 7a.
375 Afterward, the average value of REV (\overline{REV}) and associated distance (d_m) from mass
376 center to corresponding cells contained in PCE plume at $t=1523$ min are presented in Fig.
377 7a. Regression analysis is performed for average REVs of PCE plume and d_m , where fitted



378 models and associated R^2 for Experiments-I and II are listed in Table 4. Simultaneously,
379 the fitted equations between \overline{REV} and d_l (the distance from injection point to cell
380 contained in PCE plume) also are derived by regression analysis. From the results in Fig.
381 7a, \overline{REV} of S_o and A_{ow} appear a peak and then decrease with increasing of d_m and d_l for
382 Experiment-I. \overline{REV} of S_o and A_{ow} for Experiment-I all firstly increase and then decrease
383 with the increasing of d_m and d_l , while \overline{REV} of PCE plume presents apparent decreasing
384 tendency as d_m and d_l increase for Experiment-II. In addition, the value of A_{ow} -REV
385 mostly is higher than the value of S_o -REV for two experiments.

386 The mean and standard deviation of REV_s of PCE plume during 0~1523 min derived
387 by statistical analysis (Fig. 7b). Compared with REV_s of PCE plume for Experiment-I,
388 Experiment-II (F20/30 mesh translucent silica sand with higher porosity) has larger value
389 of mean and standard deviation of REV_s. Besides, the relationship between REV_s and
390 PCE saturation are fitted by regression analysis, where fitted equation and R^2 for two
391 experiments are listed in Table 5 and Fig. 7b. With increasing of PCE saturation, REV of
392 S_o appear decline trend for two experiments. However, REV of A_{ow} increases when S_o
393 increases for both two experiments (Fig. 7b). On the other hand, REV of S_o for
394 Experiment-II is higher than corresponding REV for Experiment-I, while Experiments-I
395 and II have similar values of A_{ow} -REV (Fig. 7b). These results suggest higher porosity
396 will lead to high value of S_o -REV and the relationship between REV_s of PCE plume and
397 d_m , d_l .

398 4. Conclusions

399 In this study, a new criterion χ^i is proposed to identify the REV_s of translucent porous



400 media and inner contaminant transformation based on previous criteria. The REV plateaus
401 of observation cells selected from two experiments of PCE transport are hard to judge
402 visually from the porosity and PCE saturation curves. From the REV identification effects
403 of different criteria, the REV flat plateau is difficult to identify by coefficient of variation
404 (C_v^i) and entropy dimension (DI^i), indicating the coefficient of variation (C_v^i) and entropy
405 dimension (DI^i) are not suitable for REV estimation of translucent porous media. The
406 relative gradient error (ε_g^i) can make REV plateaus of all kinds of translucent silica
407 explicit in variation curves, but random fluctuations weaken REV plateau identification. In
408 comparison with these previous criteria, the beginning and ending of the REV flat plateaus
409 could be easily and directly identified in the curves based on the new criterion χ^i ,
410 suggesting the new criterion χ^i is more convenient and effective for REV estimation. In
411 this study, REVs of porosity, density, tortuosity, and PCE plume are estimated using the
412 new criterion χ^i .

413 Statistical results of minimum REV scales quantified by new criterion χ^i reveal
414 cumulative frequencies of porosity, density and tortuosity all have smooth convex shapes.
415 Models based on Gaussian equation are built for the distribution of REV sizes of porosity,
416 density and tortuosity, which porous media with larger porosity leads to larger values of
417 mean and standard deviation for REV sizes of media properties. For REV sizes of PCE plume,
418 result suggested larger porosity lead to larger value of mean and standard deviation.
419 Regression analysis is performed to study the regularity for distribution of REV sizes, where
420 fitted relationship between REV sizes and d_m , d_l are derived for PCE plume. \overline{REV} of S_o and
421 A_{ow} firstly increase and then decrease with the increasing of d_m and d_l for Experiment-I



422 whose sandbox packed by translucent porous media with relatively lower porosity.
423 However, \overline{REV} of S_o and A_{ow} directly decrease with the increment of d_m and d_l when
424 porosity became larger for Experiment-II. Significantly, REV size of S_o presented
425 decreasing trend as S_o increases, while increasing tendency appeared for REV size of A_{ow} .
426 Through regression analysis, the fitted equations between REVs of PCE plume and PCE
427 saturation are derived for two experiments. Implications of these finding are essential for
428 quantitative investigation of scale effect of porous media and contaminant transformation.
429 The fluid migration and transform in porous media can be simulated accurately according
430 to the REV estimation results using light transmission technique and the appropriate
431 criterion χ^i .

432 **Code and data availability**

433 The codes and data for this paper are available by contacting the corresponding author at
434 jfwu@nju.edu.cn.

435 **Author contributions**

436 Ming Wu: Conceptualization, Methodology, Writing;
437 Jianfeng Wu: Conceptualization, Methodology, Writing;
438 Jichun Wu: Conceptualization;
439 Bill X. Hu: Conceptualization, Writing.



440 **Declaration of interests**

441 The authors declare that they have no known competing financial interests or personal
442 relationships that could have appeared to influence the work reported in this paper.

443

444 **Acknowledgments**

445 We acknowledge support by the National Key Research and Development Plan of
446 China (2016YFC0402800), the National Natural Science Foundation of China (41902246,
447 41730856 and 41772254), the National Natural Science Foundation of China-Xianjiang
448 Project (U1503282) and the China Postdoctoral Science Foundation (2017M622905).

449

450 **References**

451 Al-Raoush, R., and Papadopoulos, A.: Representative elementary volume analysis of
452 porous media using X-ray computed tomography, *Power Technol.*, 200, 60-77,
453 2010.

454 Al-Raoush, R.: Change in Microstructure Parameters of Porous Media Over
455 Representative Elementary Volume for Porosity, *Part. Sci. Technol.*, 30, 1-16,
456 2012.

457 Bai, L., Wang, X., Chen, Q., Ye, Y., Zheng, H., Guo, J., Yin, Y., and Gao, C.: Explaining
458 the Size Dependence in Platinum-Nanoparticle-Catalyzed Hydrogenation
459 Reactions, *Angew. Chem. Int. Ed.*, 55, 15656-15661, 2016.

460 Bob, M.M., Brooks, M.C., Mravik, S.C., and Wood, A.L.: A modified light transmission



- 461 visualization method for DNAPL saturation measurements in 2-D models, *Adv.*
462 *Water Resour.*, 31, 727-742, 2008.
- 463 Borges, J.A.R., and Pires, L.F.: Representative elementary area (REA) in soil bulk density
464 measurements through gamma ray computed tomography, *Soil Till. Res.*, 123,
465 43-49, 2012.
- 466 Borges, J.A.R., Pires, L.F., Cássaro, F.A.M., Roque, W.L., Heck, R.J., Rosa, J.A., and Wolf,
467 F.G.: X-ray microtomography analysis of representative elementary volume (REV)
468 of soil morphological and geometrical properties, *Soil Till. Res.*, 182, 112-122,
469 2018.
- 470 Bouvry, B., del Campo, L., Meneses, D.D.S., Rozenbaum, O., Echegut, R., Lechevalier,
471 D., Gaubil, M., and Echegut, P.: Hybrid methodology for retrieving thermal
472 radiative properties of semi-transparent ceramics, *J. Phys. Chem. C*, 120,
473 3267-3274, 2016.
- 474 Bradford, S.A., Vendlinski, R.A., and Abriola, L.M.: The entrapment and long-term
475 dissolution of tetrachloroethylene in fractional wettability porous media, *Water*
476 *Resour. Res.*, 35(10), 295-2964, 1999.
- 477 Brown, G.O., and Hsieh, H.T.: Evaluation of laboratory dolomite core sample size using
478 representative elementary volume concepts, *Water Resour. Res.*, 36(5), 1199-1207,
479 2000.
- 480 Corbett, P.W.M., and Jensen, J.L.: Estimating the mean permeability: how many
481 measurement do we need? *First Break*, 10(3), 89-94, 1992.
- 482 Costanza-Robinson, M.S., Estabrook, B.D., and Fouhey, D.F.: Representative elementary



- 483 volume estimation for porosity, moisture saturation, and air-water interfacial areas
484 in unsaturated porous media: Data quality implication, *Water Resour. Res.*, 47,
485 W07513, 2011.
- 486 Erning, K., Grandel, S., Dahmke, A., and Schäfe, D.: Simulation of DNAPL infiltration
487 and spreading behavior in the saturated zone at varying flow velocities and
488 alternating subsurface geometries, *Environ. Earth Sci.*, 65, 1119-1131, 2012.
- 489 Esfandiari, A., Radha, B., Wang, F.C., Yang, Q., Hu, S., Garaj, S., Nair, R.R., Geim, A.K.,
490 and Gopinadhan, K.: Size effect in ion transport through angstrom-scale slits,
491 *Science*, 358, 511-513, 2017.
- 492 Fernandes, J.S., Appoloni, C.R., and Fernandes, C.P.: Determination of the Representative
493 Elementary Volume for the study of sandstones and siltstones by X-Ray
494 microtomography, *Mater. Res.*, 15(4), 662-670, 2012.
- 495 Ghilardi, P., Kai, A.K., and Menduni, G.: Self-similar heterogeneity in granular porous
496 media at the representative elementary volume scale, *Water Resour. Res.*, 29(4),
497 1205-1214, 1993.
- 498 Gilevska, T., Passetport, E., Shayan, M., Seger, E., Lutz, E.J., West, K.A., Morgan, S.A.,
499 Mack, E.E., and Lollar, B.S.: Determination of in situ biodegradation rates via a
500 novel high resolution isotopic approach in contaminated sediments, *Water Res.*,
501 149, 632-639, 2019.
- 502 Hendrick, A.G., Erdmann, R.G., and Goodman, M.R.: Practical Considerations for
503 Selection of Representative Elementary Volumes for Fluid Permeability in
504 Fibrous Porous Media, *Transp. Porous Med.*, 95, 389-405, 2012.



- 505 Kang, Q.J., Zhang, D.X., and Chen, S.Y.: Simulation of dissolution and precipitation in
506 porous media, *J. Geophys. Res.* 108, NO. B10, 2505, doi:10.1029/2003JB002504,
507 2003.
- 508 Kim, J., and Mohanty, B.P.: Influence of lateral subsurface flow and connectivity on soil
509 water storage in land surface modeling, *J. Geophys. Res. Atmos.*, 121,704-721,
510 2016.
- 511 Lei, S., and Shi, Y.: Separate-phase model and its lattice Boltzmann algorithm for
512 liquid-vapor two-phase flows in porous media, *Phys. Rev. E*, 99, 053302, 2019.
- 513 Martínez, F.S.J., Caniego, F.J., García-Gutiérrez, C., and Espejo, R.: Representative
514 elementary area for multifractal analysis of soil porosity using entropy dimension,
515 *Nonlin. Processes Geophys.*, 14, 503-511, 2007.
- 516 Müller, C., and Siegesmund, S.: Evaluation of the representative elementary volume (REV)
517 of a fractured geothermal sandstone reservoir, *Environ. Earth Sci.*, 61, 1713-1724,
518 2010.
- 519 Niemet, M.R., and Selker, J.S.: A new method for quantification of liquid saturation in 2D
520 translucent porous media systems using light transmission, *Adv. Water Resour.*, 24,
521 651-666, 2001.
- 522 Nordahl, K., and Ringrose, P.S.: Identifying the Representative Elementary Volume for
523 permeability in heterolithic deposits using numerical rock models, *Math Geosci.*,
524 40, 753-771, 2008.
- 525 O'Carroll, D.M., Bradford, S.A., and Abriola, L.M.: Infiltration of PCE in a system
526 containing spatial wettability variations, *J. Contam. Hydrol.*, 73, 39-63, 2004.



- 527 Pereira Nunes, J.P., Blunt, M.J., and Bijeljic, B.: Pore-scale simulation of carbonate
528 dissolution in micro-CT images, *J. Geophys. Res. Solid Earth*, 121, 558-576,
529 2016.
- 530 Piccoli, I, Schjønning, P., Lamandé, M., Zanini, F., and Morari, F.: Coupling gas transport
531 measurements and X-ray tomography scans for multiscale analysis in silty soils,
532 *Geoderma*, 338, 576-584, 2019.
- 533 Razavi, M.R., Muhunthan, B., and Al Hattamleh, O.: Representative elementary volume
534 analysis of sands using x-ray computed tomography, *Geotech. Test J.*, 30(3),
535 212-219, 2007.
- 536 Rozenbaum, O., and du Roscoat, S.R.: Representative elementary volume assessment of
537 three-dimensional x-ray microtomography images of heterogeneous
538 materials: Application to limestones, *Phys. Rev. E*, 89, 053304, 2014.
- 539 Teruel, F.E., and Rizwan-uddin: Numerical computation of macroscopic turbulence
540 quantities in representative elementary volumes of the porous medium, *Int. J.*
541 *Heat Mass Transfer.*, 53, 5190-5198, 2010.
- 542 Ukrainczyk, N., and Koenders, E.A.B.: Representative elementary volumes for 3D
543 modeling of mass transport in cementitious materials, *Modelling Simul. Mater.*
544 *Sci. Eng.*, 22, 035001, 2014.
- 545 Wang, L., Mi, J., and Guo, Z.: A modified lattice Bhatnagar–Gross–Krook model for
546 convection heat transfer in porous media, *Int. J. Heat Mass Transfer.*, 94, 269-291,
547 2016.
- 548 Wang, S., Elsworth, D., and Liu, J.: A mechanistic model for permeability evolution in



549 fractured sorbing media, *J. Geophys. Res.*, 117, B06205,
550 doi:10.1029/2011JB008855, 2012.

551 Wu, M., Wu, J.F., and Wu, J.C.: Simulation of DNAPL migration in heterogeneous
552 translucent porous media based on estimation of representative elementary volum,
553 *J. Hydrol.*, 553, 276-288, 2017.

554 Wu, M., Wu, J.F., Wu, J.C., and Hu, B.X.: Effects of microarrangement of solid particles
555 on PCE migration and its remediation in porous media, *Hydrol. Earth Syst. Sci.*,
556 22, 1001-1015, 2018.

557



558 **Table 1.** Experimental conditions

Experiment	I	II
Sandbox dimensions (cm)	20×15	60×45
Packed translucent silica sand	F40/50	F20/30
Median grain diameter (mm)	0.36	0.72
Permeability (m ²)	4.25×10 ⁻¹¹	1.35×10 ⁻¹⁰
V _{PCE} (ml)	9	32
Injection rate (ml/min)	0.5	0.5

559

560



561 **Table 2.** Criteria of REV estimation

Criterion	Equation
The coefficient of variation	$C_V^i = \frac{\hat{s}}{\hat{\varphi}_i}$
entropy dimension	$DI^i \approx \frac{\sum_{j=1}^{m(i)} \mu_j(L_e) \log \mu_j(L_e)}{\log L_e}$
the relative gradient error	$\varepsilon_g^i = \left \frac{\varphi^{i+1} - \varphi^{i-1}}{\varphi^{i+1} + \varphi^{i-1}} \right \frac{1}{\Delta L}$
New criterion	$\chi^i = \frac{ \delta_{i+1} - \delta_{i-1} }{\delta_i \Delta L}$

562

563



564 **Table 3.** The fitted equations of frequency for REV of porosity, density and tortuosity

Experiment	I	II
θ -REV	$F = -2.01 \times 10^{-12} + \frac{1}{\sqrt{2\pi} \times 1.50} e^{-\frac{(\text{REV}-4.35)^2}{2 \times 1.50^2}}$ <p style="text-align: center;">($R^2=0.955$)</p>	$F = -5.30 \times 10^{-3} + \frac{1}{\sqrt{2\pi} \times 3.35} e^{-\frac{(\text{REV}-8.05)^2}{2 \times 3.35^2}}$ <p style="text-align: center;">($R^2=0.932$)</p>
ρ -REV	$F = -7.51 \times 10^{-26} + \frac{1}{\sqrt{2\pi} \times 1.14} e^{-\frac{(\text{REV}-2.89)^2}{2 \times 1.14^2}}$ <p style="text-align: center;">($R^2=0.969$)</p>	$F = -3.18 \times 10^{-12} + \frac{1}{\sqrt{2\pi} \times 1.71} e^{-\frac{(\text{REV}-2.97)^2}{2 \times 1.71^2}}$ <p style="text-align: center;">($R^2=0.989$)</p>
τ -REV	$F = -2.76 \times 10^{-15} + \frac{1}{\sqrt{2\pi} \times 1.42} e^{-\frac{(\text{REV}-3.65)^2}{2 \times 1.42^2}}$ <p style="text-align: center;">($R^2=0.774$)</p>	$F = -8.55 \times 10^{-8} + \frac{1}{\sqrt{2\pi} \times 2.15} e^{-\frac{(\text{REV}-4.30)^2}{2 \times 2.15^2}}$ <p style="text-align: center;">($R^2=0.850$)</p>

565 *F represents the frequency of REV, θ represents porosity, ρ represents density, τ

566 represents tortuosity

567

568



569 **Table 4.** The fitted equations between average value of REV and d_i , d_m

Experiment	I		II	
	S ₀ -REV	A _{ow} -REV	S ₀ -REV	A _{ow} -REV
d_m	$\overline{REV} = -1.67 \times 10^{-3} d_m^2 + 0.193 d_m + 2.72$ (R ² =0.807)	$\overline{REV} = -6.10 \times 10^{-4} d_m^2 + 5.82 \times 10^{-2} d_m + 7.20$ (R ² =0.401)	$\overline{REV} = -4.08 \times 10^{-5} d_m^2 + 1.50 \times 10^{-2} d_m + 7.54$ (R ² =0.655)	$\overline{REV} = -1.92 \times 10^{-5} d_m^2 + 4.47 \times 10^{-3} d_m + 9.46$ (R ² =0.616)
	$\overline{REV} = -1.97 \times 10^{-3} d_i^2 + 0.245 d_i + 1.12$ (R ² =0.832)	$\overline{REV} = -1.47 \times 10^{-3} d_i^2 + 0.205 d_i + 1.84$ (R ² =0.733)	$\overline{REV} = -3.94 \times 10^{-5} d_i^2 + 7.80 \times 10^{-3} d_i + 8.50$ (R ² =0.327)	$\overline{REV} = -1.92 \times 10^{-5} d_m^2 + 4.47 \times 10^{-3} d_m + 9.46$ (R ² =0.616)

570 * \overline{REV} is the average value of REV size, d_m is the distance from mass center of PCE plume
 571 to the cell contained in PCE plume, d_i is the distance from injection point to the cell
 572 contained in PCE plume
 573
 574



575 **Table 5.** The fitted relationship between REV and S_o

Experiment	I	II
	$REV = -2.13 \times \ln S_o + 0.876$	$REV = -0.961 \times \ln S_o + 1.09$
S_o -REV	$(R^2=0.466)$	$(R^2=0.415)$
	$REV = 2.27e^{2.70*S_o}$	$REV = 1.70e^{3.30*S_o}$
Aow-REV	$(R^2=0.366)$	$(R^2=0.500)$

576

577



578 **Figure Captions**

579

580 **Figure 1.** (a) System Device for acquisition of properties of translucent material; (b) The
581 infinitesimal selected from translucent porous media packed in 2D sandbox; (c)
582 Variable changes as measured scale (L) increment in conceptual curve
583 (Costanza-Robinson et al., 2011); (d) Scale effect and the cuboid image window
584 geometry.

585 **Figure 2.** (a) The system sandbox equipment of Experiment-I; (b) The system sandbox
586 equipment of Experiment-II

587 **Figure 3.** (a) The emergent light intensity, porosity, permeability and tortuosity of 2D
588 translucent silica sand for Experiments-I and II; (b) The PCE saturation of
589 Experiments-I and II during 0~1523 min and observation cells

590 **Figure 4.** (a) The change of porosity (θ), associated coefficient of variation (C_V^i), entropy
591 dimension (DI^i), the relative gradient error (ε_g^i), and new criterion- χ^i for
592 observation cells as cuboid window scale (L) increases; (b) The change of PCE
593 saturation (S_o), associated C_V^i , DI^i , ε_g^i , and χ^i for observation cells as cuboid
594 window scale (L) increases

595 **Figure 5.** (a) The distributions of minimum REV sizes of porosity, sand density and
596 tortuosity for Experiments-I and II; (b) The frequency of minimum REV sizes of
597 Experiments and fitted models

598 **Figure 6.** (a) The distributions of S_o -REV sizes during 0~1523 min for Experiments-I and
599 II; (b) The distributions of AOW-REV sizes during 0~1523 min for Experiments-I
600 and II

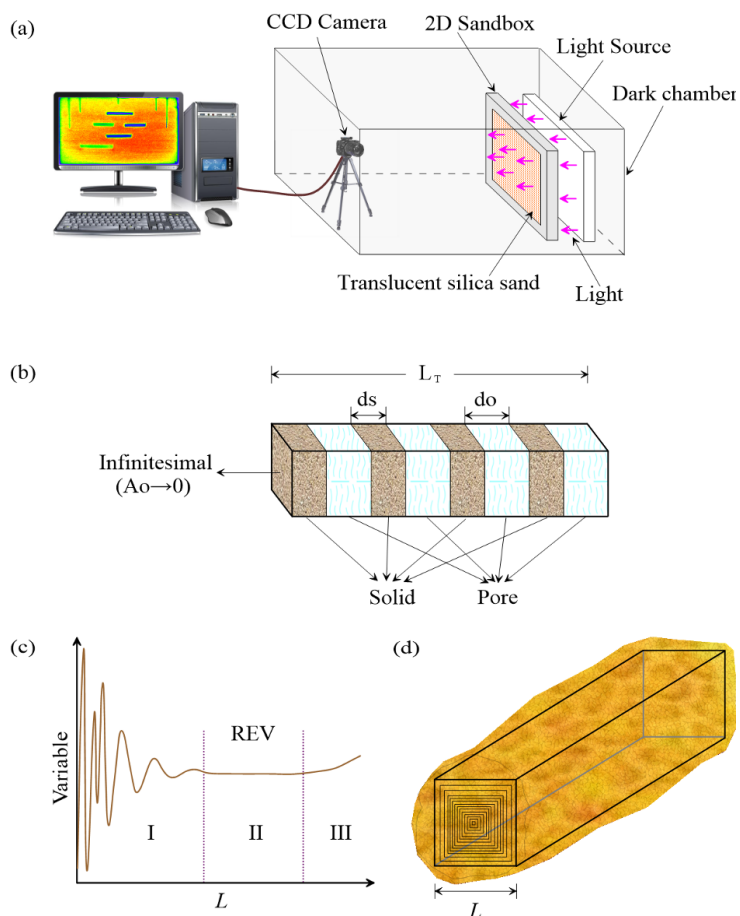


601 **Figure 7.** (a) The mass center coordinate of PCE plume and the change of average REV
602 size as the distance d_i , d_m increases; (b) The mean, standard deviation of S_o -REV
603 and A_{ow} -REV during 0~1523 min and fitted relationship between REV sizes and
604 S_o for Experiments-I and II
605



606 **Fig. 1**

607



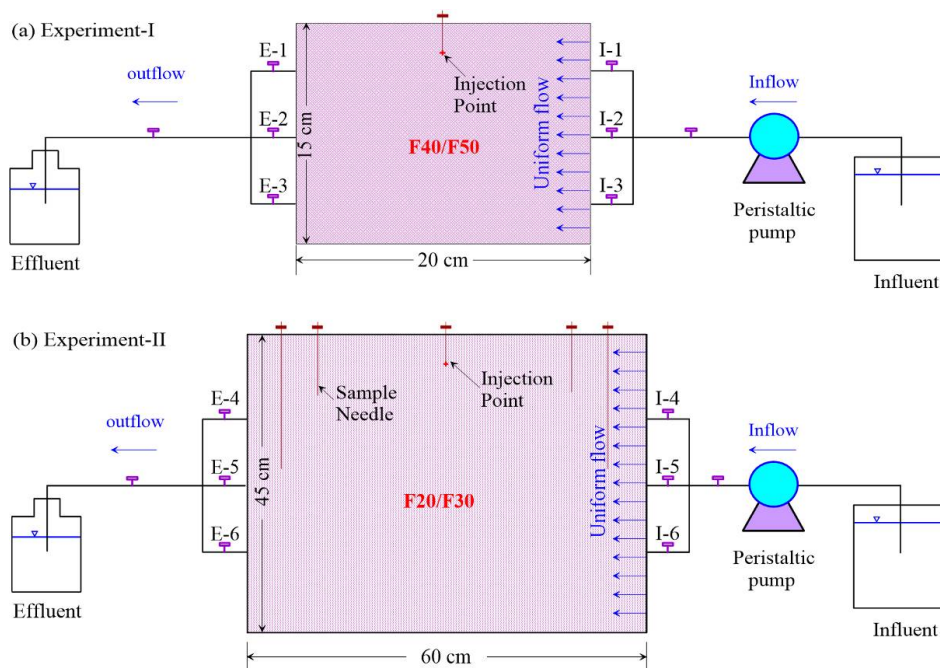
608

609



610 **Fig. 2**

611



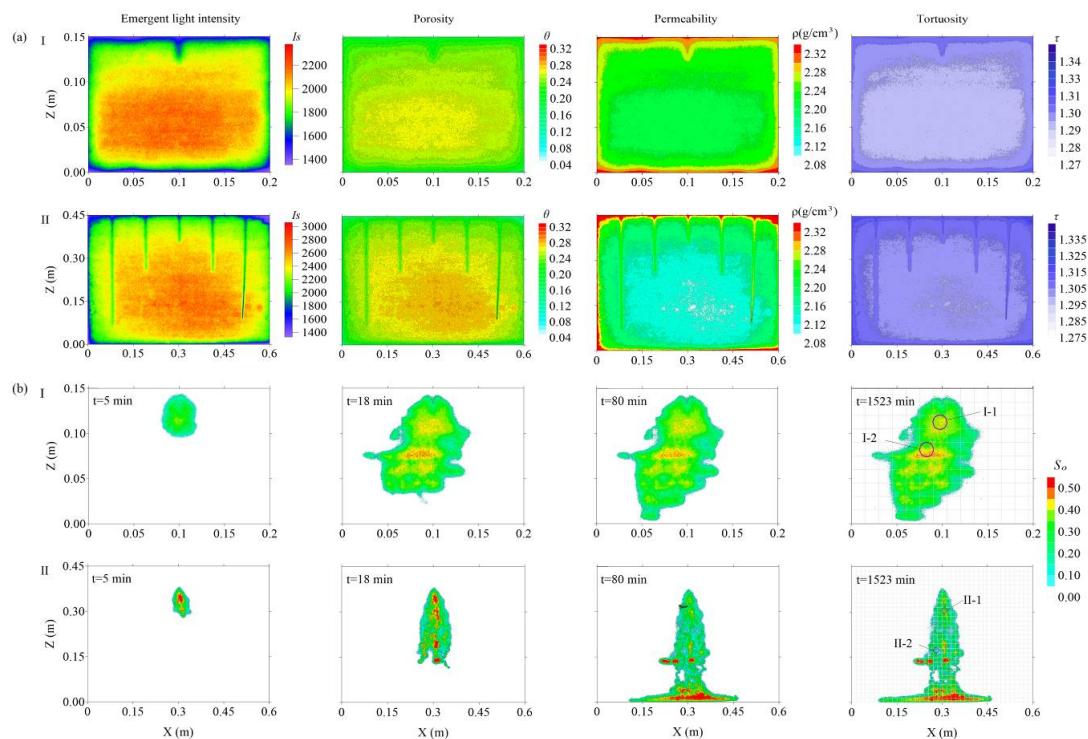
612

613



614 **Fig. 3**

615



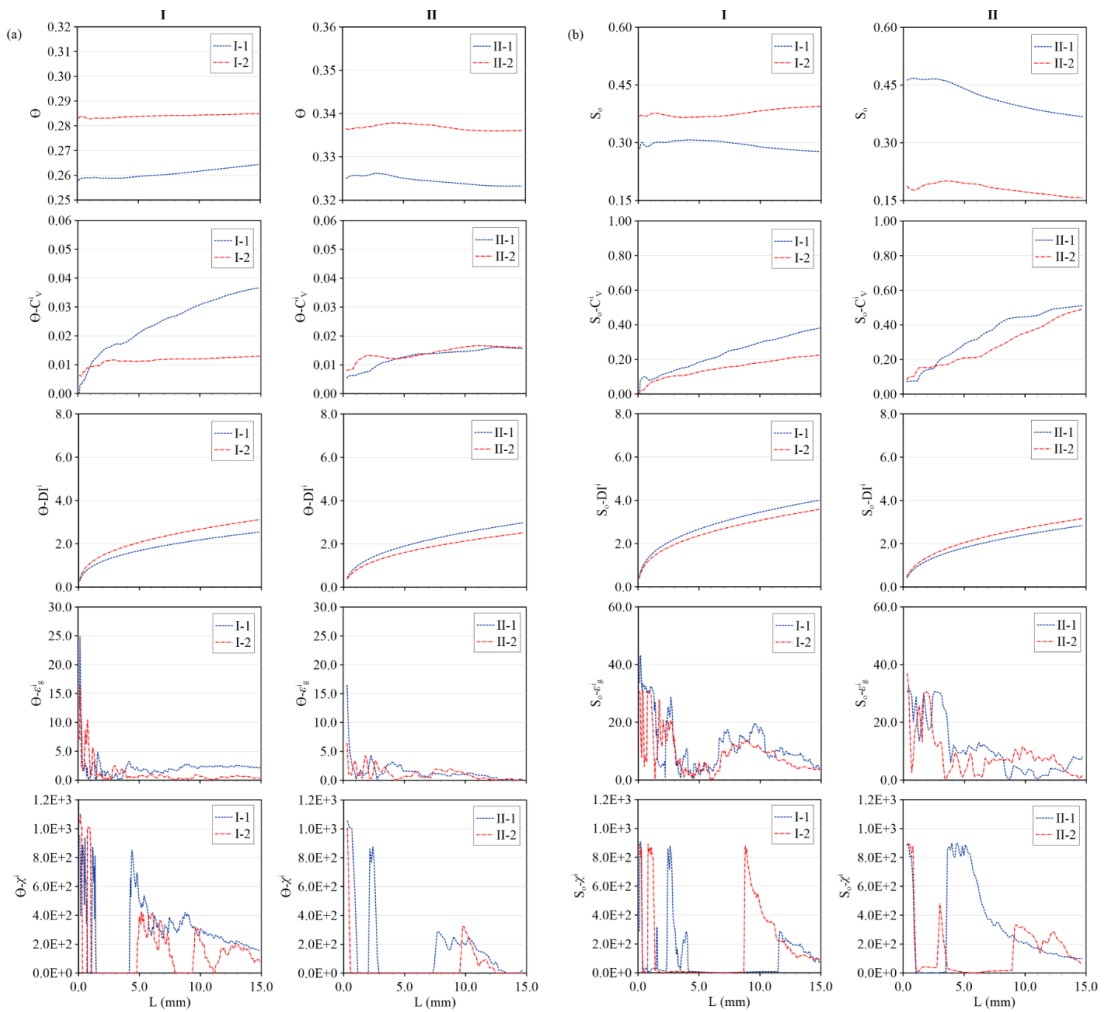
616

617



618 **Fig. 4**

619



620

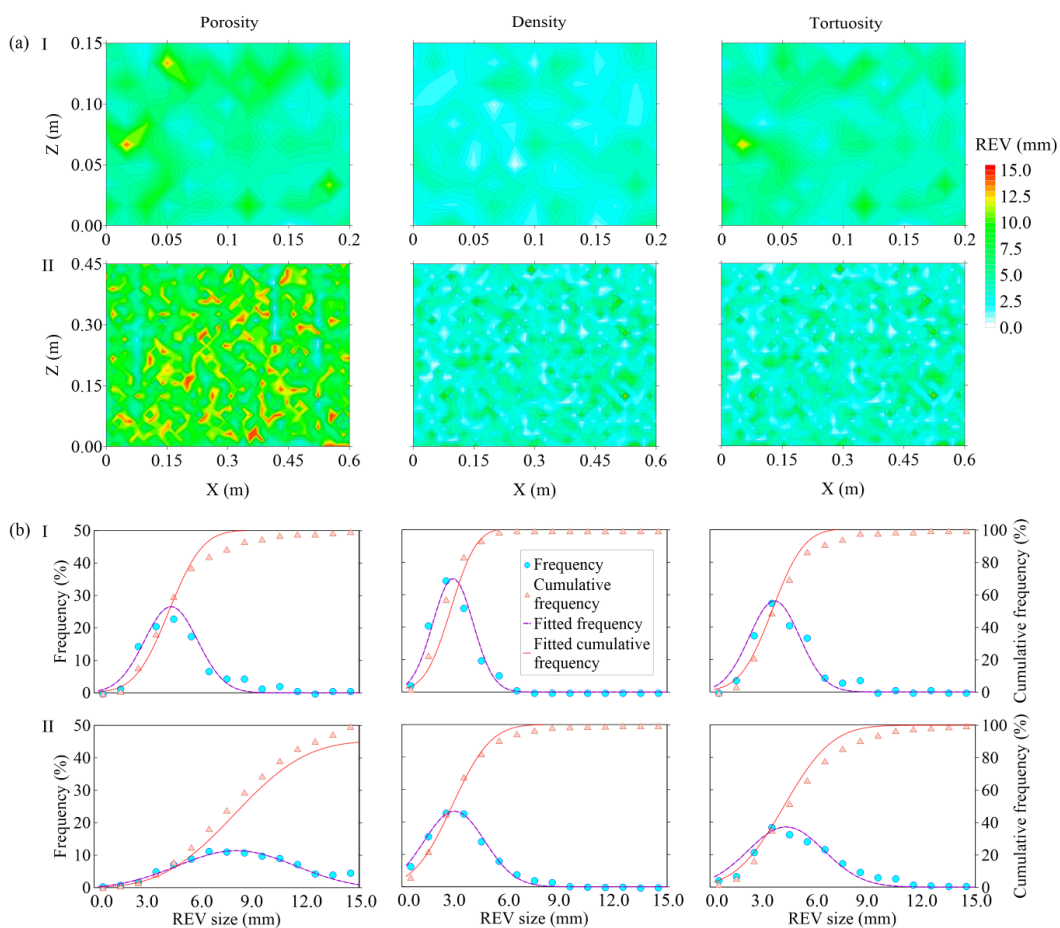
621

622



623 **Fig. 5**

624



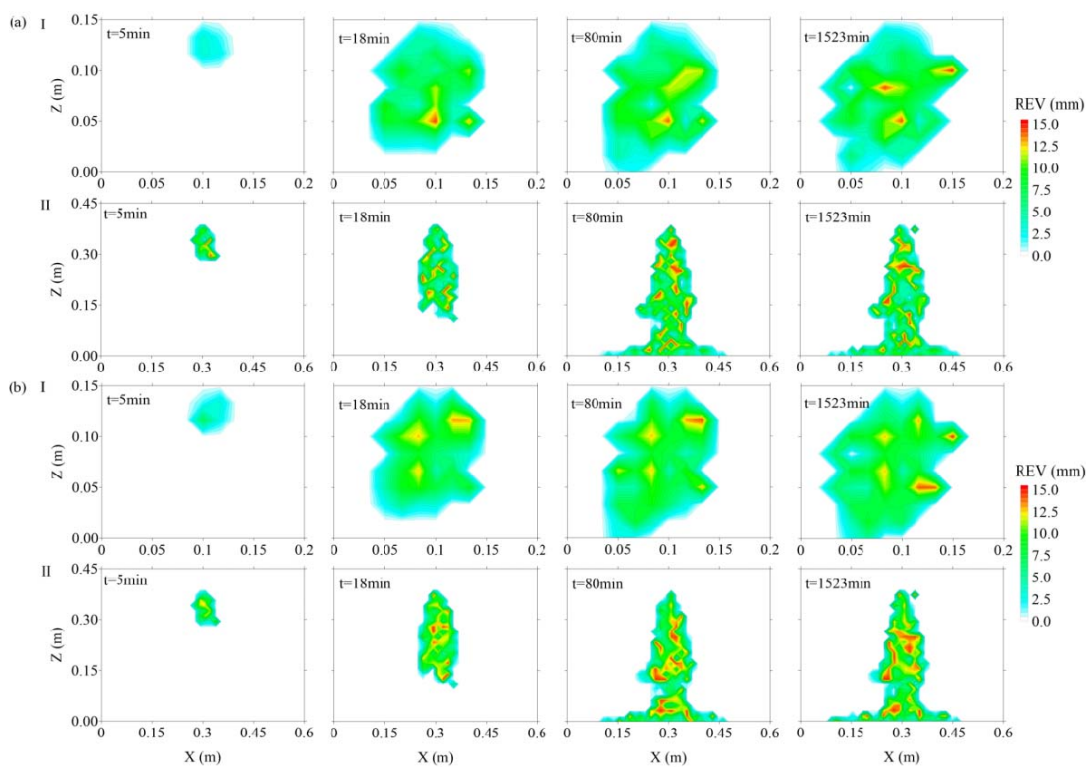
625

626



627 **Fig. 6**

628



629

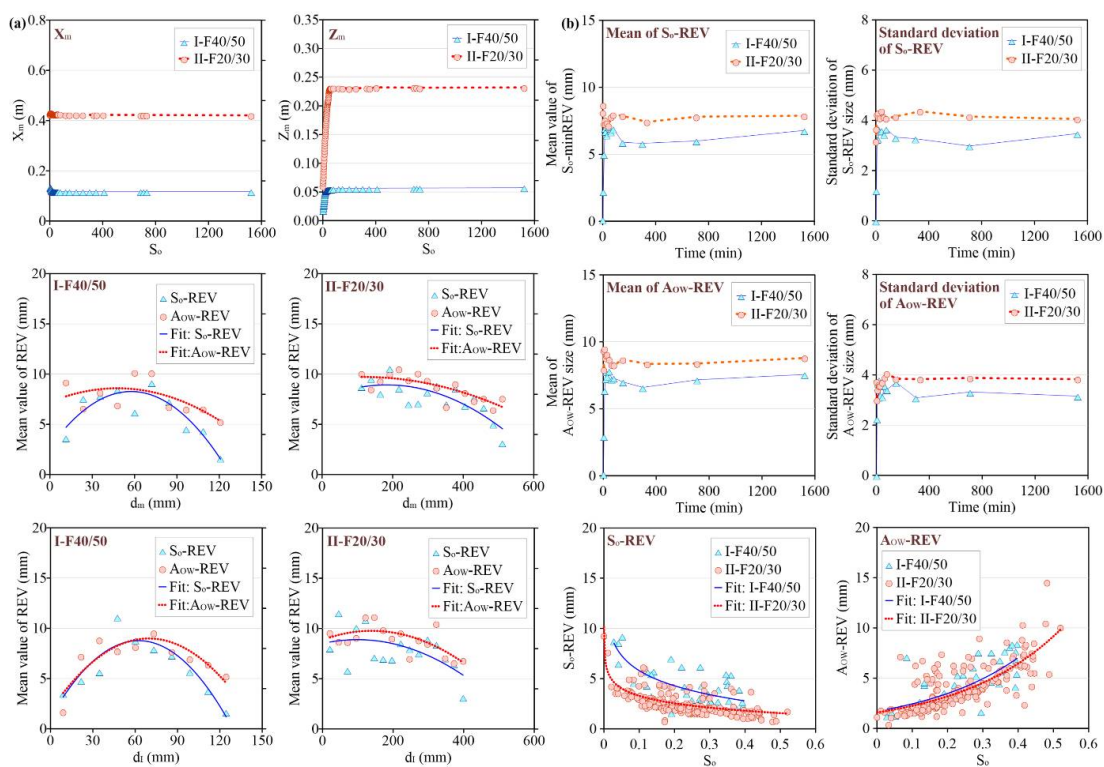
630

631



632 **Fig. 7**

633



634